Single- and double-electron capture in intermediate-energy Ar^{8+} + He collisions

Y. W. Zhang [2] J. W. Gao [1,*] Y. Wu,[3,2,†] J. G. Wang,[3] N. Sisourat,[4] and A. Dubois[4]

[1]*School of Physics, Hangzhou Normal University, Hangzhou 311121, China*

[2]*Center for Applied Physics and Technology, HEDPS, and School of Physics, Peking University, Beijing 100871, China*

[3]*Key Laboratory of Computational Physics, Institute of Applied Physics and Computational Mathematics, Beijing 100088, China*

[4]*Sorbonne Université, CNRS, UMR 7614, Laboratoire de Chimie Physique-Matière et Rayonnement, 75005 Paris, France*

(Received 25 July 2022; accepted 6 October 2022; published 14 October 2022)

Single- and double-electron-capture processes occurring in Ar^{8+} and He collisions are investigated in a broad energy domain ranging from 0.1 to 100 keV/u. Total and partial cross sections are calculated using a two-active-electron semiclassical asymptotic-state close-coupling approach. For single-electron-capture cross sections the present results show the best overall agreement with available experimental data for both total and partial cross sections, and possible reasons for observed discrepancies are discussed. Furthermore, we extend the understanding of the electron-capture processes on that system to impact energies above 20 keV/u for which no data exist. The cross sections for double-electron-capture processes are also reported and show severe discrepancies with the rare available experimental data.

DOI: 10.1103/PhysRevA.106.042809

I. INTRODUCTION

The study of electron-capture processes in the collisions of multiply charged ions with atoms has received and is still receiving a great deal of attention [1–8]. This interest has been generated to a large degree in the fields of thermonuclear fusion research and astrophysics [9–12], where the collisional properties of highly charged ions play an important role. From a fundamental perspective, the study of electron-capture processes involving multiply charged ions is also of challenging importance, especially in the intermediate-impact energy domain, as their dynamics illustrates the effects of static and dynamical electronic correlations, strong Coulombic interactions, and many-channel close-coupling schemes related to the charge asymmetry between the target and projectile. Furthermore, electron-capture studies are important for exploring collision dynamics and for aiming at the solution of few-body momentum exchange [13].

In the present work, we are interested in single- (SEC) and double-electron-capture (DEC) processes,

$$\begin{aligned} Ar^{8+} + He(1s^2) &\rightarrow Ar^{7+}(n\ell) + He^{+}(n'\ell'), \\ Ar^{8+} + He(1s^2) &\rightarrow Ar^{6+}(n\ell n'\ell') + He^{2+}, \end{aligned} \tag{1}$$

respectively, in the intermediate energy range. In fact, this collisional system was already studied theoretically and experimentally in the past [14–22]. For the SEC processes, most of the early works focused on the total and state-selective cross sections. Salzborn and Muller [14] and Justiniano *et al.* [15] measured total SEC cross sections in the energy region of 0.01–1 keV/u. Following the measurements [14,15], Kimura and Olson [16] performed molecular-orbital close-coupling (MOCC) calculations for the dominant channels, i.e., SEC to $n = 4$ final states for impact energies ranging from 0.01 to 10 keV/u; the results were in accord with the measured total SEC cross sections [14,15]. Later, Druetta *et al.* [17] and Gosselin *et al.* [18] performed state-selective cross-section measurements using vacuum ultraviolet spectroscopy and an energy-gain technique, respectively, for energies lower than 2 keV/u. Their experimental data were found to be in reasonable agreement with the results from the MOCC [16] and Landau-Zener calculations [23]. More recently, using the cold-target recoil-ion-momentum spectroscopy (COLTRIMS) technique, Zhang *et al.* [22] and Abdallah *et al.* [20] measured angular-differential cross sections for the dominant channels in Ar^{8+} and He collisions at 3 and 6.25 keV/u, respectively. In [20] the authors showed that a Landau-Zener treatment to describe the angular distributions appears to be inadequate, while the coupled-channel calculations describe better the angular distributions. Zhang *et al.* [22] also performed theoretical calculations using a single-active-electron atomic-orbital close-coupling method. However, the results were found to be in poor agreement with their measurements. For the DEC processes, experimental data are more scare and only available for energies lower than 2 keV/u [15,17]. To our knowledge, no theoretical investigation for DEC processes has been reported so far.

Despite the intensive investigation of Ar^{8+} and He collisions, a comprehensive understanding of the collision processes is still far from satisfactory, in particular for the state-selective cross sections, for which considerable discrepancies still exist between available experimental and theoretical results. Moreover, no experimental data and theoretical predictions for high impact energies exist.

In this work, we theoretically study SEC and DEC processes in Ar^{8+} + He collisions for a wide energy domain

*gaojunwen@hznu.edu.cn; gwen_32@163.com

†wu_yong@iapcm.ac.cn

ranging from 0.1 to 100 keV/u. We use a two-active-electron semiclassical asymptotic-state close-coupling (SCASCC) method, taking into account explicitly the electron-electron correlations between the two active electrons. In order to resolve the discrepancies between the measurements and calculations, comparisons are performed for both total and state-selective cross sections. Possible reasons for the existing discrepancies are also discussed.

The present paper is organized as follows. In the next section we briefly outline the SCASCC method used in the present calculations. In Sec. III, we present a detailed analysis of the total and partial cross sections for SEC and DEC processes, including direct comparisons with available experimental and theoretical results. A brief conclusion follows in Sec. IV. Atomic units are used throughout, unless explicitly indicated otherwise.

II. THEORY

In the present work, we have calculated total and partial SEC and DEC cross sections in Ar^{8+} and He collisions using a two-active-electron SCASCC approach, which was previously described, for example, in [24–27]. Here we outline only briefly the main features of the approach. The two-electron time-dependent Schrödinger equation is written as

$$\left[H - i\frac{\partial}{\partial t}\right]\Psi(\vec{r}_1, \vec{r}_2, t) = 0, \tag{2}$$

with the electronic Hamiltonian

$$H = \sum_{i=1,2}\left[-\frac{1}{2}\nabla_i^2 + V_T(r_i) + V_P\left(r_i^p\right)\right] + \frac{1}{|\vec{r}_1 - \vec{r}_2|}, \tag{3}$$

where $\vec{r}_i$ and $\vec{r}_i^{\,p} = \vec{r}_i - \vec{R}(t)$ are the position vectors of the electrons with respect to the target and the projectile, respectively. The relative projectile-target position $\vec{R}(t)$ defines the trajectory, with $\vec{R}(t) = \vec{b} + \vec{v}t$ in the usual straight-line, constant-velocity approximation, where $\vec{b}$ and $\vec{v}$ are the impact parameter and velocity, respectively (see Fig. 1). The terms V_T and V_P represent the interactions between the active electrons and the collision partners, the target and projectile, respectively, expressed as

$$V_T(r_i) = -\frac{2}{r_i}, \quad V_P\left(r_i^p\right) = -\frac{8}{r_i^p} - \frac{1}{r_i^p}\left(10 + \alpha r_i^p\right)e^{-\beta r_i^p}. \tag{4}$$

V_T corresponds to He^{2+}, and V_P corresponds to the Ar^{8+} ion in the frozen-core electron approximation in which the inner-shell electrons are assumed to be inactive. The latter is taken from [20], in which the variational parameters $\alpha = \beta = 5.5$ were optimized in order to reproduce the experimental energy of the Ar^{7+} levels.

The Schrödinger equation is solved by expanding the scattering wave function onto a basis set composed of states of the isolated collision partners,

$$\Psi(\vec{r}_1, \vec{r}_2, t) = \sum_{i=1}^{N_{TT}} a_i^{TT}(t)\Phi_i^{TT}(\vec{r}_1, \vec{r}_2)e^{-iE_i^{TT}t} + \sum_{j=1}^{N_{PP}} a_j^{PP}(t)\Phi_j^{PP}(\vec{r}_1, \vec{r}_2, t)e^{-iE_j^{PP}t}$$

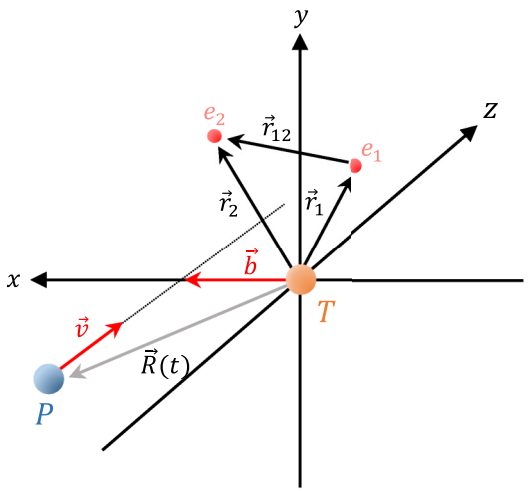

FIG. 1. Collision geometry. The impact parameter $\vec{b}$ and velocity $\vec{v}$ define the collision plane (xz) and $\vec{R}(t)$ the projectile (P) trajectory with respect to the target (T). The positions of the two electrons with respect to the target center are denoted $\vec{r}_1$ and $\vec{r}_2$, and $\vec{r}_{12}$ is the relative vector between the two electrons. Note that for clarity we locate the origin of the reference frame on the target; this does not restrict the generality of our results, which are Galilean invariant.

$$+ \sum_{k=1}^{N_T}\sum_{l=1}^{N_P} a_{kl}^{TP}(t)\left[\phi_k^T(\vec{r}_1)\phi_l^P(\vec{r}_2, t) + \phi_k^T(\vec{r}_2)\phi_l^P(\vec{r}_1, t)\right]e^{-i(E_k^T + E_l^P)t}, \tag{5}$$

where the T and TT (P and PP) superscripts denote the states and corresponding energies for which one and two electrons are on the target (projectile), respectively. Note that since the total spin state of the collision system is a singlet, the Φ_i^{TT} and Φ_j^{PP} states are singlets, and we restrict the last term in Eq. (5) to the spatial symmetric combination of one-electron states. Moreover, for both electrons, the projectile states contain plane-wave electron translation factors $e^{i\vec{v}\cdot\vec{r}_i - i\frac{1}{2}v^2 t}$, ensuring Galilean invariance of the results. The insertion of Eq. (5) into (2) results in a system of first-order coupled differential equations, which can be written in matrix form as

$$i\frac{d}{dt}\mathbf{a}(t) = \mathbf{S}^{-1}(\vec{b}, \vec{v}, t)\mathbf{M}(\vec{b}, \vec{v}, t)\mathbf{a}(t), \tag{6}$$

where $\mathbf{a}(t)$ is the column vector of the time-dependent expansion coefficients, i.e., a^{TT}, a^{PP}, and a^{TP} in Eq. (5), and $\mathbf{S}$ and $\mathbf{M}$ are the overlap and coupling matrices, respectively. These equations are solved using the predictor-corrector, variable-time-step Adams-Bashford-Moulton method for a set of initial conditions: initial state i and given values of b and v. The probability of a transition $i \to f$ is given by the coefficients a_f ($\equiv a^{TT}$, a^{PP}, or a^{TP}) as

$$P_{fi}(b, v) = \lim_{t\to\infty} |a_f(t)|^2. \tag{7}$$

The corresponding state-to-state integral cross sections for the considered transition are calculated as

$$\sigma_{fi}(v) = 2\pi\int_0^{+\infty} bP_{fi}(b, v)db. \tag{8}$$

TABLE I. Comparison of energies (in a.u.) of Ar^{7+} and Ar^{6+} ions obtained using the model potential in Eq. (4) with energies from NIST [28] E_{NIST}. The values of the energies are given relative to the Ar^{7+} first ionization threshold (ionization potential = 5.2720 a.u.), which sets the origin of our scale.

Ar^{7+}				Ar^{6+}			
State	E_{GTO}	E_{NIST}	Δ[a]	State	E_{GTO}	E_{NIST}	Δ[a]
$3s\ ^2S^e$	−5.2811	−5.2720	0.17%	$3s^2\ ^1S^e$	−9.8638	−9.8440	0.20%
$3p\ ^2P^o$	−4.6816	−4.6254	1.22%	$3s3p\ ^1P^o$	−9.1162	−9.0661	0.55%
$3d\ ^2D^e$	−3.7640	−3.7561	0.21%	$3p^2\ ^1D^e$	−8.7398	−8.6377	1.18%
$4s\ ^2S^o$	−2.6433	−2.6477	0.17%	$3p^2\ ^1S^e$	−8.4990	−8.4009	1.17%
$4p\ ^2P^e$	−2.4132	−2.4065	0.28%	$3s3d\ ^1D^e$	−8.1735	−8.1568	0.20%
$4d\ ^2D^e$	−2.0664	−2.0935	1.29%	$3p3d\ ^1D^o$	−7.8685	−7.7914	0.99%
$4f\ ^2F^o$	−2.0075	−2.0057	0.09%	$3p3d\ ^1F^o$	−7.5725	−7.5190	0.71%
$5s\ ^2S^e$	−1.5906	−1.5936	0.19%	$3p3d\ ^1P^o$	−7.5306	−7.4879	0.57%
$5p\ ^2P^o$	−1.4792	−1.4784	0.05%	$3s4s\ ^1S^e$	−7.4553	−7.4341	0.29%
$5d\ ^2D^e$	−1.3082	−1.3295	1.60%	$3s4p\ ^1P^o$	−7.2657	−7.2478	0.25%
$5f\ ^2F^o$	−1.2782	− 1.2836	0.42%	$3s4d\ ^1D^e$	−6.9460	−6.9494	0.05%
$5g\ ^2G^e$	−1.2737	−1.2806	0.53%	$3d^2\ ^1D^e$	−6.8208	−6.8069	0.20%
				$3s4f\ ^1F^o$	−6.8065	−6.8026	0.06%
				$3d^2\ ^1G^e$	−6.8410	−6.8001	0.60%
				$3p4p\ ^1P^e$	−6.7041	−6.6621	0.63%
				$3d^2\ ^1S^e$	−6.6505	−6.6198	0.46%
				$3s5s\ ^1S^e$	−6.5833	−6.5871	0.06%
				$3p4p\ ^1D^e$	−6.6117	−6.5612	0.77%
				$3s5p\ ^1P^o$	−6.4748	−6.4639	0.17%
				$3s5d\ ^1D^e$	−6.3115	−6.3222	0.17%

[a] $\Delta = |(E_{GTO} - E_{NIST})/E_{NIST}|$.

In the present calculations, a set of 92 Gaussian-type orbitals (GTOs; 12 for $\ell = 0$, 7×3 for $\ell = 1$, 4×5 for $\ell = 2$, 3×7 for $\ell = 3$, and 2×9 for $\ell = 4$) is used on the Ar^{8+} center, while 19 GTOs (10 for $\ell = 0$ and 3×3 for $\ell = 1$) are located on the He center. These two sets allow the inclusion of 5982 singlet states and pseudostates in total: 96 TT (He), 1359 TP (He^+, Ar^{7+}), and 4527 PP (Ar^{6+}) states, describing elastic, SEC, DEC, and ionization channels. Note that the SEC into $Ar^{7+}(n > 5)$ is described by pseudostates of energy lying above $Ar^{7+}(5g)$ and below the first ionization threshold of Ar^{7+}. Moreover, the DEC into higher excited states is described by pseudostates lying above $Ar^{6+}(3\ell 5\ell')$ and below the ionization threshold of Ar^{6+}, while ionization is described by pseudostates of energy lying up to 1 a.u. above ionization thresholds. In Table I, we give the energies of important Ar^{6+} and Ar^{7+} states, which are compared with the corresponding data listed in the NIST tables [28]. The overall agreement between our calculated energies and the tabulated data is generally very good and at worst equal to about 1.6% for the excited level $Ar^{7+}(5d)$.

The cross sections reported in the next section are compared with those obtained from a smaller basis set on the Ar^{8+} center built from 66 GTOs (10 for $\ell = 0$, 6×3 for $\ell = 1$, 3×5 for $\ell = 2$, 2×7 for $\ell = 3$, and 1×9 for $\ell = 4$). Total SEC and DEC cross sections from these two sets agree with each other within 5% and 10%, respectively. The $n\ell$-resolved SEC cross sections for the dominant channels [SEC into $Ar^{7+}(4\ell)$] from these two sets agree with each other within 15% in the whole considered energy region. For weak channels, i.e., SEC into $Ar^{7+}(3\ell$ and $5\ell)$, the values of the cross sections are more than one order of magnitude smaller than the dominant ones, and the convergence was found to be better than 30%, except for SEC into $Ar^{7+}(3s$ and $5s)$ at the highest considered energy (100 keV/u), where the results from two basis sets differ by up to 50%. For the double-electron capture, the cross sections of $Ar^{6+}(3\ell 3\ell')$ and $Ar^{6+}(3\ell 4\ell'$ and $3\ell 5\ell')$ production converged within 15% at worst for low energies and within 10% at intermediate and high energies. For the cross sections summed over DEC into other higher excited states (above $3\ell 5\ell'$ and below the first ionization threshold of Ar^{6+}), the convergence is better than 10%.

III. RESULTS AND DISCUSSION

A. Total single-electron-capture cross sections

In Fig. 2, our total single-capture cross sections for Ar^{8+}+ He collisions are presented in the energy region from 0.1 to 100 keV/u, together with available experimental [14,15,17] and theoretical [16] results. It should be noted that the total SEC cross sections are largely dominated (>90%) by the contribution of the pure SEC channel, i.e., $Ar^{8+} + He(1s^2) \rightarrow Ar^{7+}(n\ell) + He^+(1s)$, over the considered collision energy range. Our cross sections exhibit a plateaulike structure for energies lower than 1 keV/u, a weak maximum located at about 2 keV/u, and a rapid drop for increasing energies. The presence of a shoulder at about 40 keV/u is due to the increasing importance of the population of high-ℓ states at high impact energies, as discussed below (see Fig. 3). The MOCC calculations of Kimura and Olson [16] are seen to exceed ours by up to 70% at 10 keV/u and show a very different behavior, with cross sections decreasing slowly to

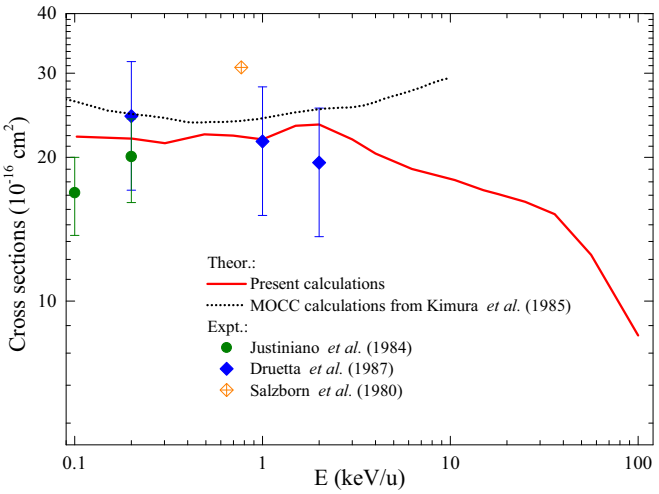

FIG. 2. Total single-electron-capture cross sections as a function of the impact energy. The present results are plotted as a red solid line; theoretical results from Kimura and Olson [16] are denoted as a black dotted line, and the experimental results of Justiniano *et al.* (the data reported in Figs. 4 and 12 of [15] for 0.1 and 0.2 keV/u, respectively), Druetta *et al.* [17], and Salzborn and Muller [14] are shown as symbols.

a minimum around 0.5 keV/u and then increasing steadily as impact energies increase. The discrepancy between the MOCC results and ours is most likely due to the very limited basis set (11 molecular states) that the authors used in their calculations at that time. On the other hand, the convergence of our total SEC cross sections was found to be about 5%, as mentioned above. In Fig. 2, we also compare our results with experimental data [14,15,17], which are available only for energies lower than 2 keV/u. These results do not agree with each other, showing a 20% difference between experimental data of [15,17] at 0.2 keV/u and a 40% difference between those of [14,17] around 1 keV/u. Our cross sections lie in between the experimental data of [15,17] and show good agreement, better than 20%, with [17]. Furthermore, we extend the cross sections to impact energies higher than 2 keV/u, for which we can compare with only the theoretical results reported up to 10 keV/u in [16]. The latter present a surprising rise, certainly due to the use of approximate electron factors (developed at first order in velocity), which might not be valid for velocities larger than 0.3 a.u. Without any other data, it is clear that further experimental and theoretical efforts are required to draw definite conclusions in this range.

B. Absolute $n\ell$-resolved single-electron-capture cross sections

We now investigate $n\ell$-resolved SEC cross sections. Such detailed information on the final-state distribution of captured electrons is of particular interest both in astrophysics and in plasma diagnostics research since it determines the characteristics of the emitted radiation.

Our absolute $n\ell$-resolved SEC cross sections for production of $Ar^{7+}(n\ell; n = 3, 4,$ and $5)$ are presented in Fig. 3, together with the available experimental [17] and theoretical [16] results. Our results in Fig. 3(d) show that the single capture into the $n = 4$ shell is the dominant channel in the whole

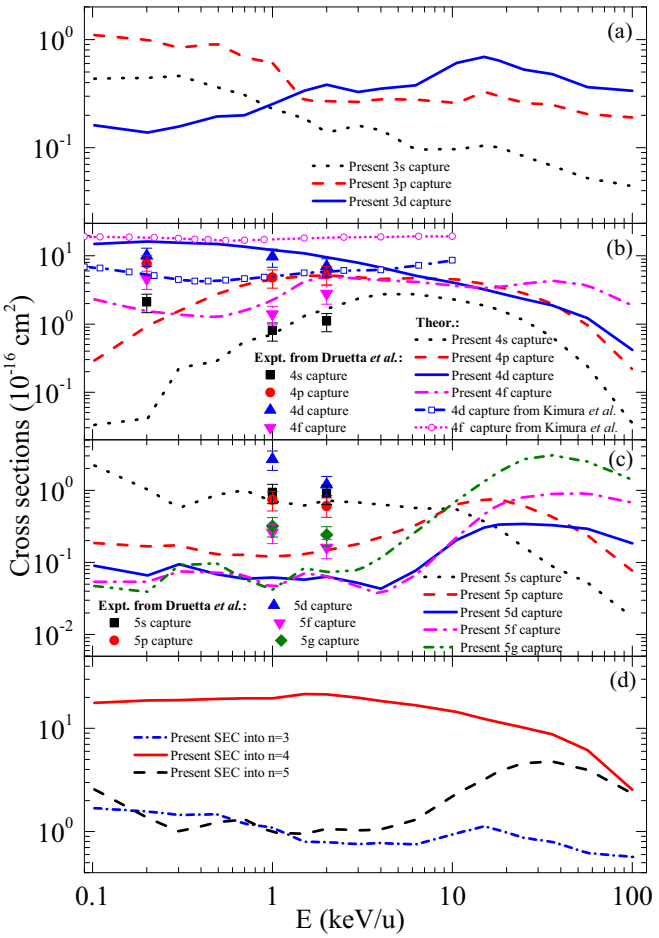

FIG. 3. The absolute n- and $n\ell$-resolved SEC cross sections as a function of impact energy for (a) $Ar^{7+}(3\ell)$, (b) $Ar^{7+}(4\ell)$, (c) $Ar^{7+}(5\ell)$, and (d) $Ar^{7+}(n = 3,$ 4, and 5). The present results are plotted as different lines; theoretical results from Kimura and Olson [16] for $4d$ and $4f$ capture are denoted as lines with open circles. The experimental results of Druetta *et al.* [17] are shown as symbols.

considered energy region, in agreement with the experimental results of [17,20,22] (see Fig. 4), as well as those reported in [19,29,30] (not shown). At low energies, the cross sections for SEC into $Ar^{7+}(n = 3)$ and $Ar^{7+}(n = 5)$ are about one order of magnitude smaller than the ones for SEC into $Ar^{7+}(n = 4)$, while at high energies the production for $Ar^{7+}(n = 5)$ is comparable to that of $Ar^{7+}(n = 4)$. It can be seen from Fig. 3(b) that SEC into $Ar^{7+}(4d)$ is dominant at low impact energies, up to about 10 keV/u, where the production of $Ar^{7+}(4p)$, that of $Ar^{7+}(4d)$, and that of $Ar^{7+}(4f)$ become comparable. The latter dominates over all other processes at higher impact energies, which we cannot compare to existing data. This behavior is in accord with the experimental results reported in [17]. However, the MOCC calculations of Kimura and Olson [16] predict dominant SEC to the $4f$ subshell, with nearly constant cross sections from 0.1 to 10 keV/u, and therefore differ significantly from our results as well as the experimental data. It should be noted that at low energies their cross sections of SEC to $4f$ are close to our $4d$ cross sections: this tendency may indicate that the avoided crossing between

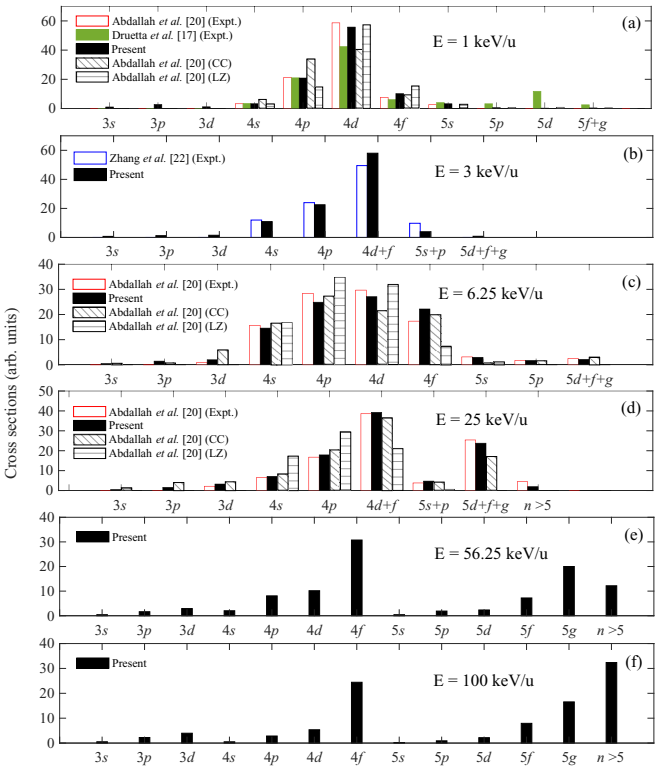

FIG. 4. Comparison of theoretical and experimental relative cross sections for SEC to various final states at impact energies of 1, 3, 6.25, 25, 56.25, and 100 keV/u. The present results are denoted by black solid bars. The experimental results are from Abdallah *et al.* [20] (red open bars), Druetta *et al.* [17] (green solid bars), and Zhang *et al.* [22] (blue open bars). The theoretical results are from Abdallah *et al.* [20] using a close-coupling (CC) method (black bars with slash lines) and the Landau-Zener (LZ) treatment (black bars with horizontal lines).

the two molecular curves related to these asymptotic levels (see Fig. 1 in [16]) may be not well described and somewhat larger than what it should be, limiting the population transfer from $4f$ to $4d$ during the collision. For SEC into $Ar^{7+}(4s)$, $Ar^{7+}(4p)$, and $Ar^{7+}(4d)$ at 1 and 2 keV/u impact energies, our results and the absolute cross sections reported in [17] are in very good agreement, within the experimental error bars, and only our cross sections for SEC into $Ar^{7+}(4f)$ are found to be significantly larger than the experimental data. However, at 0.2 keV/u, severe discrepancies exist between our results and [17], except for the dominant channel, i.e., the capture to $Ar^{7+}(4d)$. For the 5ℓ-resolved SEC cross sections presented in Fig. 3(c), our results indicate that the cross section for SEC into $Ar^{7+}(5s)$ is the largest one up to 10 keV/u, beyond which SEC into $Ar^{7+}(5g)$ takes over. It can also be seen from Fig. 3(c) that the experimental data reported in [17] for 5ℓ-resolved SEC cross sections are much larger than ours. The cause of these discrepancies can be partially attributed to systematic experimental errors related to the anisotropy of the measured emissions and the existence of a possible metastable ion fraction in the projectile beam, as discussed in that study [17]. It should be noted that the convergence of our calculations has been checked and is better than 30% for 5ℓ-resolved cross sections. Furthermore, the validity of our results is also supported by the excellent agreement with recent experimental data [20] for the relative state-resolved SEC cross sections [see Fig. 4(a)]: it therefore seems that the experimental data from Druetta *et al.* [17] underestimate the cross sections for SEC into $Ar^{7+}(4d)$ and overestimate those for $Ar^{7+}(n = 5)$.

For the 3ℓ-resolved SEC cross sections presented in Fig. 3(a), no experimental or theoretical investigations are available to our knowledge. Our results show that the productions of $Ar^{7+}(3p)$ and $Ar^{7+}(3d)$ are dominant for energies lower and higher than 1.5 keV/u, respectively. Finally, note that the relative ℓ distributions in the cross sections for SEC into $Ar^{7+}(n = 3, 4, \text{and } 5)$ presented in Fig. 3 approximately follow the statistical ℓ distribution at high impact energies, for which the electron is therefore mainly captured into subshells of the maximum ℓ. The increasing importance of the population to high-ℓ states, i.e., $Ar^{7+}(3d, 4f, \text{and } 5g)$, at high impact energies results in the shoulderlike structure observed in the total SEC cross sections (see Fig. 2).

C. Relative $n\ell$-resolved single-electron-capture cross sections

We next compare our results with the existing data for relative $n\ell$-resolved SEC cross sections, which can provide a further stringent test of the calculations. In Fig. 4, our relative cross sections for SEC to various final states are presented at impact energies of 1, 3, 6.25, 25, 56.25, and 100 keV/u. The available previous experimental [17,20,22] and theoretical [20] results are also displayed for comparison. Note that the cross sections are normalized to a total of 100 for each impact energy. From Fig. 4, one can observe the contribution of the different state-selective capture processes to the total SEC. At 1 and 3 keV/u, the experimental results [20,22] show that the cross section for SEC into $4d$ is dominant over those of $4p$, $4f$, $4s$, and $5s$. As the impact energy increases, the contributions of both $4f$ and $4s$ states become important, and a strong population of the $n = 5$ state can be observed at 25 keV/u. Our results are generally in very good agreement with the experimental data [20,22] and reproduce well the behavior of the contribution for different state-selective capture processes. Compared with the available theoretical calculations [20], our results are in agreement with coupled-channel calculations from [20] for impact energies of 6.25 and 25 keV/u. However, at the lowest impact energies (1 keV/u), the coupled-channel calculations underestimate the cross sections for the dominant channel, SEC into $Ar^{7+}(4d)$, and overestimate those for $Ar^{7+}(4p)$. The disagreement is probably due to the single-active-electron approximation used in [20] and therefore the effects of the second electron and of the electronic correlation. It should also be noted that the results shown in Fig. 4 indicate that the Landau-Zener treatment is inadequate to describe accurately the final-state distribution of the capture electrons in the present collision system. For higher impact energies, for which no other data are available, our results show that the population of high-n states increases rapidly and that, for each n shell, the electrons are mostly captured in the subshell of the largest ℓ.

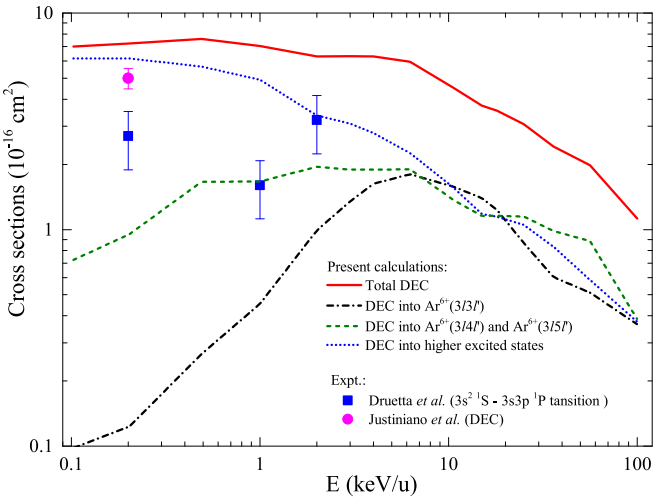

FIG. 5. Total and partial DEC cross sections are presented as a function of impact energy. The present results are plotted as lines, and the experimental results of Druetta *et al.* [17] and Justiniano *et al.* (the data reported in Fig. 12 of [15]) are shown as symbols.

D. Total and partial double-electron-capture cross sections

In Fig. 5, our cross sections for the total and partial DEC processes are presented, together with the rare available experimental data, i.e., the results reported in [15,17]. A behavior similar to SEC is seen for DEC, with a weak dependence of the cross sections for energies ranging from 0.1 to about 6 keV/u. However, these results are about a factor of 3 smaller at low energies and about one order of magnitude smaller at high energies. Our calculations show that double-capture processes to the lowest levels of Ar^{6+} and, notably, the equivalent-electron configuration $3\ell 3\ell'$ are non-negligible only at high impact energies, above about 7 keV/u, where they are of comparable importance to DEC to higher excited states (above $3\ell 5\ell'$ and below the first ionization threshold of Ar^{6+}). Then at energies above 20 keV/u, the production of the nonequivalent-electron configurations $3\ell n\ell'$ ($n = 4$ and 5) become dominant. However, at low energies the double-capture processes into higher excited states are totally dominant; their related cross sections exceed by one order of magnitude those of production of the $3\ell 4\ell'$ and $3\ell 5\ell'$ levels.

Large discrepancies exist between the available experimental data [15,17] and the present results. The experimental data of Justiniano *et al.* [15] at 0.2 keV/u are about 30% lower than our total DEC cross sections. This discrepancy may be due to the existence of the possible metastable ion fraction in the projectile beam as discussed in [15] since, in general, electron-capture cross sections related to metastable ions differ from those for the corresponding ground-state ions. However, taking these collision events into account would require the composition of the Ar^{8+} beam (the nature of the metastable states and their proportions with respect to the ground state) as well the detailed geometry of the apparatus used in [15] to account for the possible decay of the metastable projectile when reaching the collision zone. These important details are not given in [15], so it would be extremely speculative to quantify the effect of those collisional events. The data of Druetta *et al.* [17] stem from vacuum ultraviolet spectroscopy and correspond to the cross sections of the 58.5-nm line, i.e., the emission of the $3s^2\ ^1S$-$3s3p\ ^1P$ transition. However, our cross sections for DEC into $Ar^{6+}(3\ell 3\ell')$ are much smaller than the experimental data [17]. We cannot make a firm conclusion on that issue, although the convergence of the present calculation has been checked, as mentioned above, to be about 15% for the cross sections of DEC into $Ar^{6+}(3\ell 3\ell')$.

IV. CONCLUSION

In this work, single- and double-electron-capture processes occurring in the course of Ar^{8+} and He collisions have been investigated using a two-active-electron, two-center, semiclassical asymptotic-state close-coupling approach over a wide collision energy range. For single-electron-capture processes, our results show the best overall agreement with the available experimental data for both total and partial cross sections. Possible reasons for observed discrepancies were also discussed. Furthermore, our work provides a set of single-electron-capture cross sections for impact energies up to 100 keV/u. We found that the relative ℓ distributions in the cross sections for single-electron capture into $Ar^{8+}(n = 3, 4,$ and 5) follow approximatively the statistical weight related to the angular momentum ℓ at high impact energies. The increasing importance of the population to high-ℓ states, i.e., $Ar^{7+}(3d, 4f,$ and $5g)$, at high impact energies was observed as a shoulderlike structure around 40 keV/u in the total single-electron-capture cross sections.

In contrast to single-electron capture, there are large discrepancies between our results and the rare existing experimental results for the double-electron-capture cross sections. Our calculations indicated that double-electron capture into high excited states is dominant at low energies, while these processes become of comparable magnitude and strongly coupled to DEC into $Ar^{6+}(3\ell 3\ell')$ and into $Ar^{6+}(3\ell n\ell')$ ($n = 4$ and 5) at high energies.

Our work provides data for these electronic processes, which are essential to improve our understanding of this relevant collision system. However, further experimental and theoretical investigations on single- and double-electron-capture processes are needed to confirm our predictions and draw definite conclusions.

ACKNOWLEDGMENTS

This work is supported by the National Natural Science Foundation of China (Grants No. 11934004 and No. 12004350), the startup project from Hangzhou Normal University, and the Key Laboratory of Computational Physics of Institute of Applied Physics and Computational Mathematics (Grant No. 6142A05QN21001).

[1] H. F. Beyer and V. P. Shevelko, *Introduction to the Physics of Highly Charged Ions*, Series in Atomic Molecular Physics (Institute of Physics, Bristol, 2003).

[2] F. J. Currell, *The Physics of Multiply and Highly Charged Ions*, Vol. 1, *Sources, Applications and Fundamental Processes* (Springer, Dordrecht, The Netherlands, 2003).

[3] R. Janev and H. Winter, Phys. Rep. **117**, 265 (1985).

[4] M. Barat and P. Roncin, J. Phys. B **25**, 2205 (1992).

[5] T. J. M. Zouros, B. Sulik, L. Gulyás, and K. Tőkési, Phys. Rev. A **77**, 050701(R) (2008).

[6] F. Aumayr *et al.*, J. Phys. B: At. Mol. Opt. Phys. **52**, 171003 (2019).

[7] I. Madesis, A. Laoutaris, T. J. M. Zouros, E. P. Benis, J. W. Gao, and A. Dubois, Phys. Rev. Lett. **124**, 113401 (2020).

[8] D. S. La Mantia, P. N. S. Kumara, S. L. Buglione, C. P. McCoy, C. J. Taylor, J. S. White, A. Kayani, and J. A. Tanis, Phys. Rev. Lett. **124**, 133401 (2020).

[9] *Atomic Processes in Basic and Applied Physics*, edited by H. T. Viacheslav Shevelko, Springer Series on Atomic, Optical, and Plasma Physics Vol. 68 (Springer, Berlin, 2012).

[10] H. W. Drawin, Phys. Scr. **24**, 622 (1981).

[11] T. E. Cravens, Science **296**, 1042 (2002).

[12] L. Gu, J. Kaastra, and A. Raassen, Astron. Astrophys. **588**, A52 (2016).

[13] *Ion-Atom Collisions: The Few-Body Problem in Dynamic Systems*, edited by M. Schulz (De Gruyter, Berlin/Boston, 2019).

[14] E. Salzborn and A. Muller, in *Proceedings of the XIth International Conference on the Physics of Electronic and Atomic Collisions Kyoto, 1979*, edited by N. Oda and K. Takayanagi (North Holland, Amsterdam, 1980) Note that the data were reported in Ref. [16].

[15] E. Justiniano, C. L. Cocke, T. J. Gray, R. Dubois, C. Can, W. Waggoner, R. Schuch, H. Schmidt-Böcking, and H. Ingwersen, Phys. Rev. A **29**, 1088 (1984).

[16] M. Kimura and R. E. Olson, Phys. Rev. A **31**, 489 (1985).

[17] M. Druetta, S. Martin, T. Bouchama, C. Harel, and H. Jouin, Phys. Rev. A **36**, 3071 (1987).

[18] A. Gosselin, D. Hennecart, X. Husson, H. Kucal, D. Leeler, A. Lepoutre, A. Cassimi, J. P. Grandin, P. Jardin, and C. Adjouri, J. Phys. B **28**, 445 (1995).

[19] S. Bliman, M. Cornille, B. A. Huber, and J. F. Wyart, Phys. Rev. A **56**, 4683 (1997).

[20] M. A. Abdallah, W. Wolff, H. E. Wolf, E. Sidky, E. Y. Kamber, M. Stöckli, C. D. Lin, and C. L. Cocke, Phys. Rev. A **57**, 4373 (1998).

[21] G. Schenk and T. Kirchner, J. Phys. B **42**, 205202 (2009).

[22] R. T. Zhang, X. L. Zhu, X. Y. Li, L. Liu, S. F. Zhang, W. T. Feng, D. L. Guo, Y. Gao, D. M. Zhao, J. G. Wang, and X. Ma, Phys. Rev. A **95**, 042702 (2017).

[23] L. Benmeuraien, in *Proceedings of the 15th International Conference on Physics of Electronic and Atomic Collisions* (Brighton, UK, 1987), p. 557.

[24] N. Sisourat, I. Pilskog, and A. Dubois, Phys. Rev. A **84**, 052722 (2011).

[25] J. W. Gao, Y. Wu, N. Sisourat, J. G. Wang, and A. Dubois, Phys. Rev. A **96**, 052703 (2017).

[26] Y. W. Zhang, J. W. Gao, Y. Wu, F. Y. Zhou, J. G. Wang, N. Sisourat, and A. Dubois, Phys. Rev. A **102**, 022814 (2020).

[27] J. W. Gao, Y. Y. Qi, Z. H. Yang, Z. M. Hu, Y. W. Zhang, Y. Wu, J. G. Wang, A. Dubois, and N. Sisourat, Phys. Rev. A **104**, 032826 (2021).

[28] A. Kramida, Yu. Ralchenko, J. Reader, and NIST ASD Team, NIST Atomic Spectra Database, version 5.9, https://physics.nist.gov/asd.

[29] A. Bordenave-montesquieu, P. Benoit-Cattin, M. Boudjema, A. Gleizes, and S. Dousson, Nucl. Instrum. Methods Phys. Res., Sect. B **23**, 94 (1987).

[30] R. Hutton, M. H. Prior, S. Chantrenne, M. H. Chen, and D. Schneider, Phys. Rev. A **39**, 4902 (1989).